A Multifrequency Electron Spin Resonance Study of T4 Lysozyme Dynamics Using the Slowly Relaxing Local Structure Model

Zhichun Liang, Yan Lou, and Jack H. Freed*

Baker Laboratory of Chemistry and Chemical Biology, Cornell University, Ithaca, New York 14853-1301

Linda Columbus and Wayne L. Hubbell

Jules Stein Eye Institute and Department of Chemistry and Biochemistry, University of California, Los Angeles, California 90095-7008

Received: April 6, 2004; In Final Form: August 3, 2004

Electron spin resonance (ESR) spectra were obtained at 250 and 9 GHz for nitroxide-labeled mutants of the protein T4 lysozyme in aqueous solution over a range of temperatures from 2 to 37.5 °C. Two mutants labeled at sites 72 and 131 were studied and compared. The mutant sites are solvent exposed and free of tertiary interactions with other side chains, but the former is at the center of a 5 turn helix, whereas the latter site is on a small two and a half turn helix. The 250 GHz ESR spectra, because of their "fast time scale", are rather insensitive to the slow overall tumbling motion of the protein. Thus, they are qualitatively different for the two mutants, implying that there are different local dynamics at the two sites. The 9 GHz spectra, which are significantly affected by the overall tumbling and are less sensitive to the internal dynamics, do not show such marked differences between the two sites. The 250 and 9 GHz spectra for each mutant and temperature were simultaneously fit to the slowly relaxing local structure (SRLS) model for slow-motional ESR, using newly developed software. The SRLS model explicitly accounts for the overall tumbling of the protein and the internal modes of motion, which include the motion of the nitroxide side chain (expected to be the same for both mutants) and backbone fluctuations. Very good simultaneous fits are obtained. Whereas two conformers (or spectral components) are typically detected at the lower temperatures, only a single component is observed at the higher temperatures. The significant differences in the high-frequency spectra for the two mutants are readily attributed mainly to a difference in their respective local ordering. That is, site 72 exhibits significantly greater local ordering than does site 131, which is expected from the greater rigidity of the larger helix on which the 72 site is located. The results of this multifrequency study are compared with a previous 9 GHz study. A description of the application of the SRLS model in such a multifrequency study is provided.

1. Introduction

The dynamic modes of proteins include the overall rotation of the protein, backbone fluctuations, internal motions of the side chains, and conformational switching, all of which may be important for protein function.[1−3] In principle, site-directed spin-labeling (SDSL) can provide quantitative data on each of these modes.[4−7] In this technique, a nitroxide side chain is substituted at a selected site, and the dynamic behavior of the nitroxide can be deduced from a proper analysis of the ESR spectrum.[8] A basic premise of SDSL experiments aimed at elucidating protein dynamics is that the motion of the nitroxide encodes information on all of the dynamic modes of the protein. A current goal in SDSL research is to develop strategies to extract that information.

Significant progress has been made toward this goal for the nitroxide side chain designated R1 (Figure 1) at helix surface sites in T4 lysozyme (cf. Figure 2). In recent studies, dynamic contributions from the overall rotational diffusion mode of the protein were reduced by increasing the solution viscosity, and contributions from the internal modes of the side chain,[4] and backbone fluctuations were characterized.[7] In these studies, the motion of the nitroxide was analyzed using the microscopically ordered but macroscopically disordered (MOMD) model.[9] In this model the nitroxide diffusion is constrained by a local ordering potential (microscopically ordered), but the globular protein is immobilized on the ESR time scale and is statically distributed with respect to the magnetic field (macroscopically disordered).

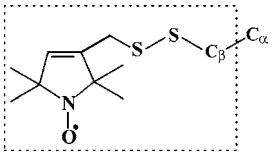

Figure 1. Structure of the R1 side chain.

An attractive alternative model for analyzing the nitroxide motion in spin-labeled proteins is the slowly relaxing local structure model (SRLS).[10−13] In this model, the overall rotational diffusion mode of the protein is accounted for explicitly, eliminating the need for increasing the viscosity of the medium. In an earlier study of T4 Lysozyme dynamics in solutions of low viscosity,[13] it was demonstrated that ESR spectra measured at 250 and 9 GHz could not be fit with the MOMD model using the same set of parameters. Because the dynamic parameters do not depend on the microwave frequency, it is clear that the

* Corresponding author.

10.1021/jp0484837 CCC: $27.50
Published on Web 10/15/2004

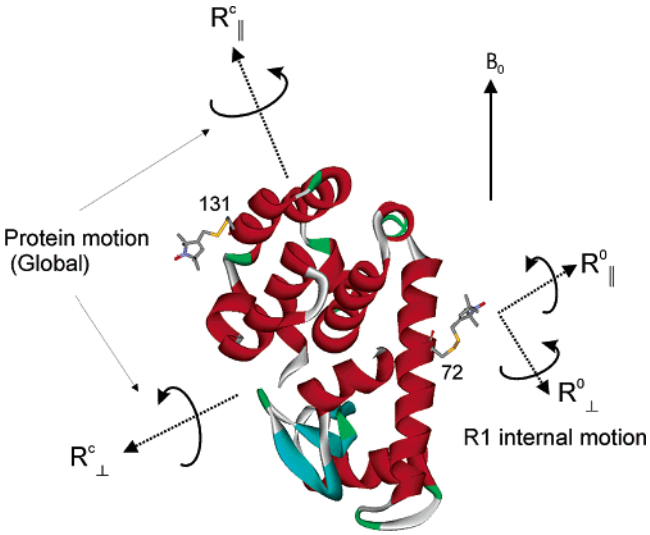

Figure 2. Ribbon model of T4 lysozyme showing the R1 side chain at sites 72 and 131. The dynamic parameters of the SRLS model are indicated (see text).

MOMD model is not adequate for analyzing multifrequency data for small proteins where rotational diffusion of the protein makes significant contributions to the nitroxide motion. In fact, it was shown that in order to fit the results at both frequencies one must explicitly account for both the global motion of the protein and the internal motion of the nitroxide side chain using the SRLS model.

The SRLS model, which was originally proposed to interpret ESR spectra for other types of systems,[10−12] has more recently been formulated in the context of ESR[8] and NMR[14] analyses of biological macromolecules. In such a slow-motional ESR study,[8] the applicability of the SRLS model and its relevant limiting models for the analysis of dynamical properties of biological systems was discussed. This model has been used to interpret experimental ESR data from spin-labeled DNA,[15] T4 lysozyme,[13] and lipid membranes,[16] and these applications have been reviewed elsewhere.[17,18] It has also been used in the analysis of protein NMR relaxation data.[19−22]

Compared with the MOMD model, more experimental data are needed to determine the larger number of fitting parameters associated with the SRLS model. One approach is to use the global diffusion constant estimated from independent experiments or from hydrodynamic theory. Then only the internal motional parameters are varied in the nonlinear least-squares (NLLS) fitting process.[23] This approach has been used in a study of the dynamical properties of DNA systems using 9 GHz ESR and hydrodynamic theory.[15] A more common approach is to use the ESR data measured at different frequencies. Multifrequency ESR has proven to be a useful tool for analyzing complex dynamics processes in biological systems. By opening multiple ESR windows, the various modes of motion with different time scales may be selectively probed and separated.[13,16−18] Multifrequency ESR has also been employed to study the rotational dynamics of a spin-labeled polymer[24] and a spin-labeled protein,[25] but without the benefit of the SRLS model. Instead, the ESR data measured at different magnetic fields were analyzed in terms of the MOMD model. Again, the spectra at different frequencies could not be simultaneously fit with the same set of parameters.

Different ESR frequencies are sensitive to motions of different time scales. This has been utilized to simplify the ESR spectral analysis. For example, when the global motion is slow enough to be in the rigid limit, the SRLS model reduces to the MOMD model. (On the other hand, if the internal motion is very fast so that it effectively partially averages the magnetic tensors, then the SRLS model reduces to the fast internal motion (FIM) model.[8]) Past work has shown that the MOMD model is often a useful approximation at 250 GHz because the global motion of the protein is too slow to substantially affect the 250 GHz spectrum. However, for small proteins at 9 GHz both the global motion and the internal dynamics affect the spectrum. Its analysis thus requires the more complex SRLS model. In this spirit, the discrepancy between the results from the 250 and 9 GHz spectral fitting was resolved in a previous multifrequency ESR study of T4 lysozyme.[13] The 250 GHz spectra were first fit using the MOMD model, and the results provided the internal motional parameters. These parameters were then used in the SRLS model fit of the 9 GHz spectra to yield the global motional rate. (From this viewpoint, it is clear that the simple MOMD model fits to the 9 GHz spectra yield results that are a composite of the internal and the overall motions but are not easily reconciled into these respective modes.[8,16]) In this work, a more general approach to extracting dynamic information from spin-labeled proteins without the use of increased solution viscosity is applied. The ESR spectra measured at the different frequencies are fit simultaneously using the SRLS model with a common set of dynamical and ordering parameters, using newly developed nonlinear least-squares fitting software. This approach does not require any assumptions regarding the time scales and their separation. It also allows for an arbitrary number of multifrequency ESR spectra to be fit simultaneously to enhance the spectral sensitivity to the fitting parameters. This method is applied to the analysis and interpretation of the dynamical behavior of T4 lysozyme mutants. Nonlinear least-squares fitting is performed to minimize the difference between the SRLS model line shapes and the experimental spectra at both 250 and 9 GHz. The focus in this work is on a comparison of the results obtained for the spin-labeled mutants 72R1 and 131R1, where R1 is free of tertiary interactions with other side chains.[4]

Perhaps most significant in this study is the dramatic sensitivity of the high-frequency, 250 GHz spectra to the subtle differences in the internal motional features at the different sites. This is illustrated in Figure 3a, which compares the 250 GHz spectra of 72R1 and 131R1 at the same temperature. These spectra are qualitatively different, despite the fact that the nitroxide label and the overall tumbling rates are identical. This clearly implies that there is different local dynamics at these two sites. The 9 GHz spectra from these two sites, on the other hand, do not show such significant differences (cf. Figure 3b). This arises for two reasons. First, given the "slower time scale" of the 9 GHz spectra, they are more substantially affected by the common overall tumbling motion.[8,13,17] Second, 250 GHz spectra provide much better orientational resolution; viz., one can clearly distinguish the precise molecular orientation corresponding to the different spectral regions in the rigid limit spectra.[17] This leads to enhanced sensitivity to the details of the internal motional dynamics of the nitroxide in the slow-motional region.[8,17]

The results are discussed in terms of the respective molecular structures and the various dynamic modes at these two sites. The major conclusions are the following: (1) At both sites, there is only one spectral component at higher temperatures, whereas at lower temperatures, two components are found, indicating a stronger interaction of the nitroxide with nearby groups in the protein. (2) The nitroxide has similar local mobilities at both sites; however, it shows a higher local ordering for 72R1 than for 131R1, most likely due to contributions from backbone

motions. For 72R1, R1 is at the center of a five turn helix, which should be more constrained in its internal motion than for 131R1, wherein R1 is on a small two and a half turn helix.

In the following section the theoretical foundations are briefly reviewed. The SRLS model is outlined within the site directed spin-labeling context, and the basis sets and their pruning, which speeds up the spectral simulations and fitting, are noted. The experimental methods are presented in section 3. In section 4, the fitting procedures and results are described. They are analyzed and discussed in section 5. Finally, the major conclusions of this work are summarized in section 6.

2. Theoretical Foundation

An ESR signal from a nitroxide spin-label located in a magnetic field, B_0, is determined in large part by the spin Hamiltonian:[28]

$$\hat{H} = \sum_{\mu=g,A} \sum_{l=0,2} \sum_{m=-l}^{l} \sum_{m'=-l}^{l} \hat{A}^{(l,m)}_{\mu,L} \mathscr{D}^{l}_{mm'}(\Omega_{LG}) F^{(l,m')*}_{\mu,G} \qquad (1)$$

In this equation, two coordinate systems, the *L* and *G* frames, have been defined: The laboratory (*L*) frame is defined with its *z*-axis along the magnetic field B_0, and the magnetic tensor (*G*) frame (more precisely the *g*-tensor frame) is determined by the molecular structure of the nitroxide. While the spin operators, $\hat{A}^{(l,m)}_{\mu,L}$, are quantized in the space-fixed *L* frame, the magnetic tensor of type μ (Zeeman or hyperfine), $F^{(l,m')}_{\mu,G}$, is best expressed in the molecule-fixed *G* frame. The Wigner rotation matrix elements relating the *L* and *G* frames, $\mathscr{D}^{l}_{mm'}(\Omega_{LG})$, are time-dependent. It is through the Euler angles, Ω_{LG}, which relate the *G* frame to the *L* frame, that the various rotational motions will affect the ESR line shapes. This transformation may be decomposed into a series of subtransformations, depending on the system under study and the model which is used.

2.1. SRLS Model. Let us consider a system where the nitroxide spin-label is attached to a macromolecule such as a protein, as illustrated in Figure 2 for T4 Lysozyme. The orientation of the nitroxide with respect to the magnetic field is modulated not only by the reorientation of the nitroxide (internal motions) but also by the overall rotation of the macromolecule (global motion). The local motion of the nitroxide is constrained by its surroundings, by its tether to the protein backbone, and by backbone flexibility. Thus, in the SRLS model we are dealing with at least two modes of motion, which we can represent by two bodies whose motions are coupled.[12] For each motion, two tensor frames need to be introduced. The first is the diffusion frame which is a body-fixed frame and is usually determined by its geometric shape. The second is the director frame whose axes represent the preferred orientation of the body. We describe this model below and note the simplifications we introduce for convenience and feasibility in fitting the experimental results.

For the internal motion of the nitroxide, the internal diffusion (*M*) frame (cf. Figure 4) is fixed with respect to the nitroxide, such that its *z*-axis is usually taken as the effective axis for internal rotation about its tether. In general, the reorientation of the nitroxide spin-label is restricted due to limited torsional oscillations about the bonds that connect it to the backbone and any interactions with the local environment. The spin-label experiences an increased orienting potential when its Z_M axis deviates from its equilibrium orientation relative to the local protein structure. This equilibrium orientation is referred to as the internal director (*C*′) frame.

The global motion of the macromolecule is frequently approximated as that of a cylinder, such that the long axis of the cylinder is taken to be the *z*-axis for the global diffusion (*C*) frame. The *C* frame is fixed in the macromolecule. In the case of a protein rotating in an isotropic solution (e.g., a water-soluble protein), the global director is arbitrary (but a membrane protein would have a preferential orientation of its *C* frame with respect to the global director).

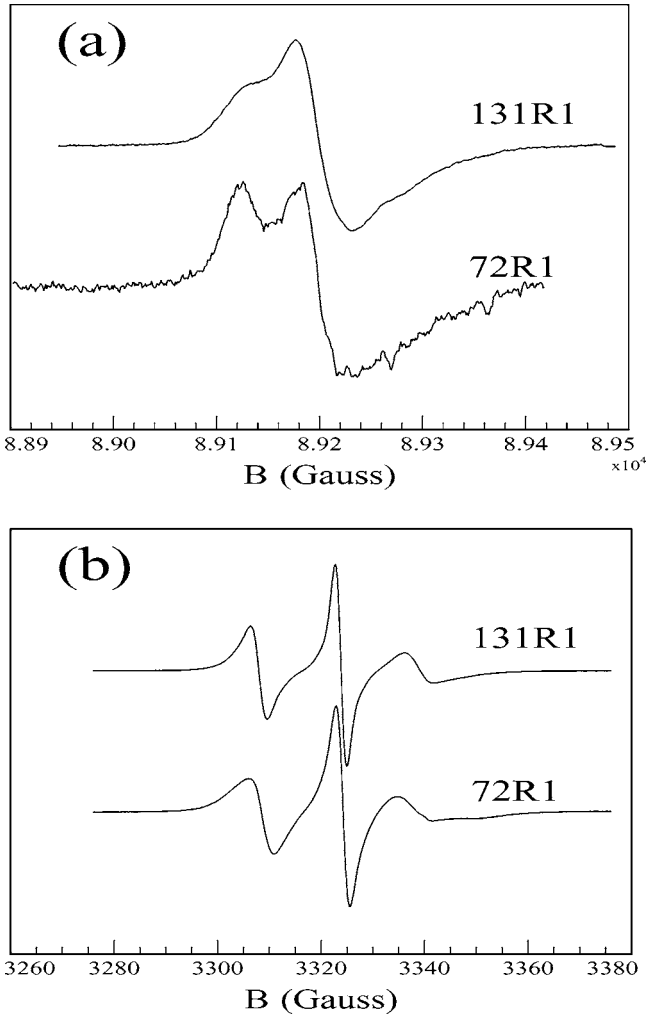

Figure 3. Comparison of the experimental ESR spectra for mutant 131R1 and 72R1 at 22 °C: (a) 250 GHz; (b) 9 GHz.

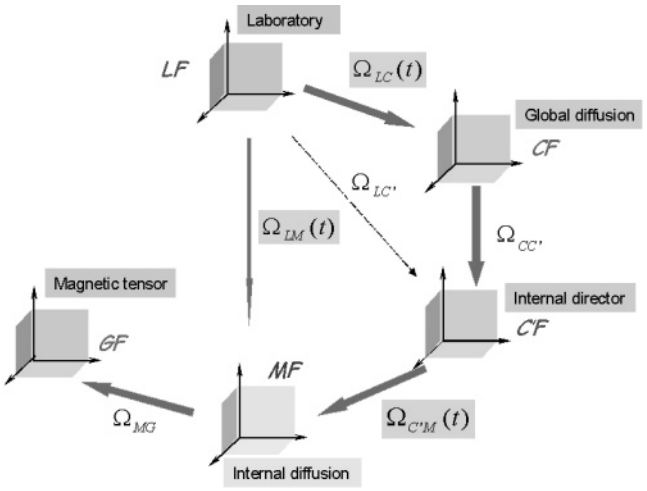

Figure 4. Various reference frames which define the slowly relaxing local structure (SRLS) and microscopic order and macroscopic disorder (MOMD) models.

The various reference frames defined in this paper and their relationships are shown in Figure 4. The lab or *L* frame is space-fixed, both the *C* and the *C′* frames are protein-fixed, and both the *M* and the *G* frames are fixed with respect to the nitroxide moiety. Thus, the Euler angles Ω_{MG} are time-independent for a rigid spin-label. It is often assumed for convenience that $\Omega_{MG} = (0, \beta_{MG}, 0)$; i.e., only the polar angle β_{MG}, also known as diffusion tilt, needs to be considered. Similarly, the Euler angles $\Omega_{CC'}$ are also time-independent for a rigid macromolecule. It is reasonable to assume that only the polar angle $\beta_{CC'}$ (cage tilt) is important. (The cage tilt may be conveniently set to zero for a spherical macromolecule.) The time-dependent Euler angles Ω_{LM} and Ω_{LC} are modulated by the internal motion and the global motion, respectively. These angles are properly referred to the fixed lab frame for purposes of properly describing the diffusion (cf. eq 3). (Note that Ω_{LM} involves the sum of rotations: $\Omega_{LC} + \Omega_{CC'} + \Omega_{C'M}$ (cf. Figure 4).) Finally, the time-dependent Euler angles $\Omega_{C'M}$ are influenced by the presence of the internal orienting potential, which couples the two modes of motion.

For the SRLS model, the spin Hamiltonian in eq 1 can be written as

$$\hat{H}_{\mathrm{SRLS}} = \sum_{\mu=g,A}\sum_{l=0,2}\sum_{m=-l}^{l}\sum_{m'=-l}^{l}\sum_{m''=-l}^{l}\sum_{m'''=-l}^{l}\sum_{m''''=-l}^{l} \hat{A}^{(l,m)}_{\mu,L}\mathscr{D}^{l}_{mm'}(\Omega_{LC})\mathscr{D}^{l}_{m'm''}(\Omega_{CC'})\mathscr{D}^{l}_{m''m'''}(\Omega_{C'M})\mathscr{D}^{l}_{m'''m''''}(\Omega_{MG})F^{(l,m'''')*}_{\mu,G} \quad (2)$$

Such a complex process of two coupled modes of motion may be described in terms of a composite diffusion operator of Ω_{LM} and Ω_{LC}:[12]

$$\hat{\Gamma}_{\mathrm{SRLS}} = \hat{\Gamma}^{\mathrm{o}}(\Omega_{LM}) + \hat{\Gamma}^{\mathrm{c}}(\Omega_{LC}) + F^{\mathrm{o}}(-\Omega_{C'M}) + F^{\mathrm{c}}(-\Omega_{C'M}) \quad (3)$$

Here the first two terms represent the diffusive contribution from the internal motion and the global motion in an isotropic medium, respectively. For a rodlike spin probe whose internal dynamics may be approximated (in the absence of a potential) as axially symmetric, the first term takes the following form

$$\hat{\Gamma}^{\mathrm{o}}(\Omega_{LM}) = R^{\mathrm{o}}_{\perp}\,\hat{\mathbf{J}}^{\mathrm{o}2} + (R^{\mathrm{o}}_{\parallel} - R^{\mathrm{o}}_{\perp})\hat{\mathbf{J}}^{\mathrm{o}2}_{z} \quad (4)$$

where $\hat{\mathbf{J}}^{\mathrm{o}2}$ is the vector operator which generates an infinitesimal rotation of the probe and $\hat{\mathbf{J}}^{\mathrm{o}2}_{z}$ is its *z*-component. $\hat{\mathbf{J}}^{\mathrm{c}2}$ and $\hat{\mathbf{J}}^{\mathrm{c}2}_{z}$ which appear in the next equations are the equivalent operators for the cage.[12] In eq 4 two diffusion constants have been introduced: $R^{\mathrm{o}}_{\parallel}$ is related to the motion of the spin probe around its symmetry axis (Z_M), and $R^{\mathrm{o}}_{\perp}$ is related to the motion perpendicular to this symmetry axis. A similar equation holds for the global motion, but if a spherical shape is assumed for the macromolecule, $R^{\mathrm{c}}_{\perp} = R^{\mathrm{c}}_{\parallel} = R^{\mathrm{c}}$ and the second term in eq 3 becomes

$$\hat{\Gamma}^{\mathrm{c}}(\Omega_{LC}) = R^{\mathrm{c}}\hat{\mathbf{J}}^{\mathrm{c}2} \quad (5)$$

where R^{c} is the diffusion contant for the global motion.

The last two terms in eq 3 are the contributions from the internal orienting potential. They are related to the internal potential by

$$F^{\mathrm{o}} = \frac{1}{2}[R^{\mathrm{o}}_{\perp}(\hat{\mathbf{J}}^{\mathrm{o}2}u(\Omega_{C'M})) + (R^{\mathrm{o}}_{\parallel} - R^{\mathrm{o}}_{\perp})(\hat{\mathbf{J}}^{\mathrm{o}2}_{z}u(\Omega_{C'M}))] - \frac{1}{4}[R^{\mathrm{o}}_{\perp}(\hat{\mathbf{J}}^{\mathrm{o}}_{+}u(\Omega_{C'M}))(\hat{\mathbf{J}}^{\mathrm{o}}_{-}u) + R^{\mathrm{o}}_{\parallel}(\hat{\mathbf{J}}^{\mathrm{o}}_{z}u(\Omega_{C'M}))^2] \quad (6)$$

and

$$F^{\mathrm{c}} = \frac{1}{2}R^{\mathrm{c}}\Big[(\hat{\mathbf{J}}^{\mathrm{c}2}u(\Omega_{C'M})) - \frac{1}{2}(\hat{\mathbf{J}}^{\mathrm{c}}_{+}u(\Omega_{C'M}))(\hat{\mathbf{J}}^{\mathrm{c}}_{-}u(\Omega_{C'M})) - \frac{1}{2}(\hat{\mathbf{J}}^{\mathrm{c}}_{z}u(\Omega_{C'M}))^2\Big] \quad (7)$$

Here the dimensionless (or reduced) internal orienting potential, $u(\Omega_{C'M})$, is defined in terms of the actual orienting potential $U(\Omega_{C'M})$ devided by $k_{\mathrm{b}}T$ as

$$-u(\Omega_{C'M}) \equiv -U(\Omega_{C'M})/k_{\mathrm{b}}T = c_{20}\mathscr{D}^{2}_{00}(\Omega_{C'M}) + c_{22}[\mathscr{D}^{2}_{02}(\Omega_{C'M}) + \mathscr{D}^{2}_{0-2}(\Omega_{C'M})] \quad (8)$$

where two dimensionless potential coefficients have been introduced: c_{20} is a measure of the orientational ordering of the spin probe with respect to the internal director, whereas c_{22} measures the asymmetry of the ordering around the director.

A convenient measure of the orientational ordering of the spin probe is provided by the order parameters:[15]

$$S_{20} = \langle \mathscr{D}_{00}{}^{2}[\Omega_{C'M}(t)]\rangle \quad (9)$$

$$S_{22} = \langle \mathscr{D}_{02}{}^{2}[\Omega_{C'M}(t)]\rangle + \langle \mathscr{D}_{0-2}{}^{2}[\Omega_{C'M}(t)]\rangle \quad (10)$$

which may be related to the orienting potential, and hence to c_{20} and c_{22}, via the ensemble averages

$$\langle \mathscr{D}^{2}_{0n}[\Omega_{C'M}(t)]\rangle = \frac{\int \mathrm{d}\Omega\ \mathscr{D}^{2}_{0n}(\Omega)\exp(c_{20}\mathscr{D}^{2}_{00}(\Omega) + c_{22}[\mathscr{D}^{2}_{02}(\Omega) + \mathscr{D}^{2}_{0-2}(\Omega)])}{\int \mathrm{d}\Omega\exp(c_{20}\mathscr{D}^{2}_{00}(\Omega) + c_{22}[\mathscr{D}^{2}_{02}(\Omega) + \mathscr{D}^{2}_{0-2}(\Omega)])} \quad (11)$$

One may convert to Cartesian ordering tensor components according to $S_{zz} = S_{20}$; $S_{xx} = (1/2)\sqrt{3/2}S_{22} - (1/2)S_{20}$; $S_{yy} = -(1/2)\sqrt{3/2}S_{22} - (1/2)S_{20}$; note $S_{xx} + S_{yy} + S_{zz} = 0$.

Given the spin Hamiltonian in eq 1 and the diffusion operator in eq 3, the slow-motional ESR line shape can be calculated from the stochastic Liouville equation (SLE), which yields[26−28]

$$I(\omega) = \pi^{-1}\langle\langle v|[(\hat{\Gamma} - i\hat{H}^{x}) + i\omega I]^{-1}|v\rangle\rangle \quad (12)$$

From the above discussion, $I(\omega)$ may be expressed as the following function:

$$I(\omega) = I(R^{\mathrm{o}}_{\perp}, R^{\mathrm{o}}_{\parallel}, R^{\mathrm{c}}, c_{20}, c_{22}, \beta_{\mathrm{MG}}, \omega) \quad (13)$$

Therefore, the parameter space of the SRLS model used in this work consists of three motional parameters, $R^{\mathrm{o}}_{\perp}$, $R^{\mathrm{o}}_{\parallel}$, and R^{c}, two ordering parameters, c_{20} and c_{22}, and one structural parameter, β_{MG}. In the limit $R^{\mathrm{c}} \rightarrow 0$ the SRLS model reduces to the MOMD model with one fewer fitting parameter.

2.2. Basis Sets. To calculate the slow-motional ESR spectrum from eq 12, a proper basis set has to be used to represent the effects of the spin Hamiltonian given by eq 1 and the coupled diffusive motion given by eq 3. It should be a direct product of the sub-basis sets for the individual degrees of freedom. For the SRLS model, the basis set is a direct product of the subsets for the electron spin, for the nuclear spin, for the internal motion, and for the global motion, which is described in ref 12.

Whereas in principle, we need an infinite number of basis vectors, in practice, the spectrum is accurately represented with a finite number of basis vectors.[26−28] In the development of the

analysis of slow-motional ESR, a very important method has been designed to determine the minimum truncated set.[27,28] In the process of pruning the basis set, we first determine the maximum contribution of each basis vector to the ESR line shape across the whole field range. If this maximum contribution is smaller than a cutoff value, then the corresponding basis vector can be removed from the basis set. This procedure yields the minimum truncated set. It considerably reduces the dimension of the basis set. This greatly speeds up the NLLS spectral fitting, where the spectrum has to be calculated many times.

2.3. Multifrequency Fitting Procedures. Now let us consider the analysis of the dynamic properties of biomolecules, by the use of ESR spectra obtained at different frequencies (the ordering and dynamic parameters do not depend on the magnetic field). By proper choice of these frequencies, we may expect to deconvolute the different modes of motion and determine the relevant parameters with high accuracy as described above.

In an earlier approach,[13] ESR spectra measured at 250 and 9 GHz were fit separately. The 250 GHz ESR line shapes of nitroxide are sensitive to motions in the range of 10^8-10^{12} s^{-1}. On the other hand, the 9 GHz ESR line shapes are sensitive to motions in the range of 10^6-10^{10} s^{-1}, i.e., 2 orders of magnitude slower. The global motion usually has a diffusion rate of around 10^7 s^{-1}, which is typically at least 1 order of magnitude slower than the internal motion. So if we open an "ESR window" with a 250 GHz time scale, the global motion will appear to be very slow. In other words, 250 GHz ESR is mainly sensitive to the internal motion. On the basis of this consideration, it was assumed that the global motion is in the rigid limit on the 250 GHz ESR time scale, so the MOMD model was used to fit the 250 GHz spectra. The fitting generated the dynamic parameters for the internal motion. On the other hand, since 9 GHz ESR is sensitive to both the internal and the global motion, the more complex SRLS model was used to fit the 9 GHz spectra after fixing the internal dynamic parameters obtained from the 250 GHz MOMD fits. Only the global motion was varied to obtain the best fit to the 9 GHz spectra. The results then generated the dynamic parameters for the global motion. In this way, the two modes of motion were decomposed and their parameters were determined.

In the current approach of multifrequency data analysis, ESR spectra at different frequencies are fit simultaneously. There are two reasons for simultaneous multifrequency fits. First, the global motion is found to have small but significant effects on the 250 GHz ESR spectra, especially at and above room temperature, such that the parameters obtained for the internal motions show some significant differences when a SRLS model (including overall motions) is used vs a MOMD model (frozen overall motion). So it would be best to fit the ESR spectra at both frequencies with the SRLS model. Second, simultaneous fitting improves the statistics, thereby improving the experimental precision of the parameters for the internal motions, which make important contributions to both the 9 and 250 GHz spectra. Additionally, in any future studies utilizing a wider range of frequencies between 9 and 250 GHz (e.g., 95 and 170 GHz available in our laboratory), both global and internal motions will be important at the intermediate frequencies, requiring the SRLS model.

We have therefore developed new software for simultaneously fitting the ESR spectra measured at different frequencies.[29] However, it should be noted that such fitting will in general be time-consuming since the global motion is extremely slow on the high-frequency ESR time scale. Thus, the basis set needed for a SRLS fit of the high-frequency spectra becomes extremely large. The pruning procedure described in the previous subsection is therefore very useful in reducing the matrix dimension and speeding up the fitting. Since the pruned basis set is usually much larger for a high-frequency spectral fit than for a low-frequency one, different pruned basis sets should be used for fitting spectra at different frequencies.

Since the computation of high-frequency ESR spectra is time-consuming, it is appropriate to ask how a SRLS computation compares with that for the simpler MOMD model wherein the overall motion is frozen. It is necessary, of course, to also prune a MOMD basis set to maximize its efficiency in fitting. After pruning respective SRLS and MOMD basis sets, we find that the actual SRLS computation is at most only about a factor of 2 slower for typical parameters in this study. This is undoubtedly because the MOMD calculation is slowed down by having to repeat the spectral calculation for many (ca. 40) overall orientations of the protein to produce the final spectrum, whereas in SRLS the overall motion of the protein is automatically accounted for, and the Lanczos algorithm utilized in the computation[27,28] very efficiently seeks out the solution.

In a simultaneous multifrequency fitting, the software first reads in the ESR data of the different frequencies. The pruned basis sets are then imported for the corresponding frequencies. All the motional and ordering parameters are independent of the magnetic fields, but the inhomogeneous line broadening could be a function of the field (e.g., *g*-strain contributions), which is allowed in the fitting. Finally all the parameters of both the internal motion and the global motion are varied to minimize the difference between the spectral fit and the experiment, i.e., the reduced χ^2:

$$\chi^2 = \frac{1}{N_{\text{total}} - N_{\text{parameter}}} \sum_{j=1}^{N_{\text{frequency}}} \sum_{i=1}^{N_{\text{data}}} \left[\frac{(\text{data}_i - \text{simulation}_i)^2}{\sigma_i^2} \right]_j \tag{14}$$

where N_{total} is the total number of data points of all frequencies, $N_{\text{parameter}}$ is the total number of fitting parameters, and σ_i are the estimated errors of the data points.[23]

3. Experimental Section

Two mutants of T4 lysozyme are studied here. One is 131R1, and the other is 72R1 (cf. Figure 2). The sample concentrations are 2.4 and 1.4 mM, respectively.

For the 9 GHz ESR, 6 μL of sample was placed in a 0.8 mm i.d. quartz capillary. For the 250 GHz high-field ESR, 1 μL of sample was placed in a flat quartz plate sample holder.[30] ESR spectra were taken at 2, 10, 22, and 37.5 °C. The experimental spectra at 250 GHz were adjusted to correct for a small admixture of dispersion signal, according to the procedure described by Earle et al.[31]

To obtain the hyperfine (*A*) tensor and *g* tensor components, the (near) rigid limit spectra at 9 and 250 GHz were produced in the following way. Sucrose was added to the T4 lysozyme solution until it was 63 wt % sucrose, and the viscosity was about 100 cP at room temperature. The 250 GHz spectra of these samples were taken at 10 °C, and the 9 GHz spectra were taken at liquid nitrogen temperature.

Nonlinear least-squares (NLLS) fits were performed for the 250 and 9 GHz spectra, using the general slow-motional program,[23] in the manner described previously.[13] As previously pointed out, the 250 GHz spectra are particularly sensitive to the *g* tensor fits, whereas the 9 GHz spectra provide the needed sensitivity to the *A* tensor.[13,31] In this near-rigid limit, the spectra are not very sensitive to the motional model, so simple Brownian

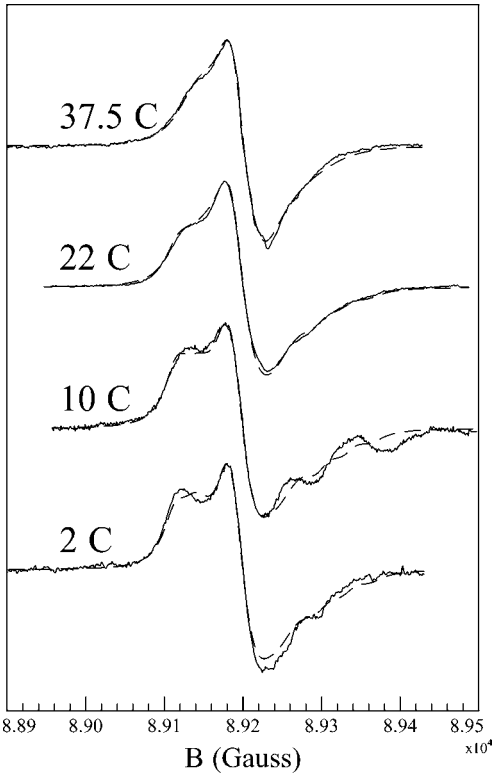

Figure 5. Nonlinear least-squares (NLLS) fits of the two-site SRLS model (dashed lines) to the experimental spectra (solid lines) at 250 GHz of T4 lysozyme in solution, spin-labeled at position 131. The best parameters from multifrequency fits are presented in Table 3.

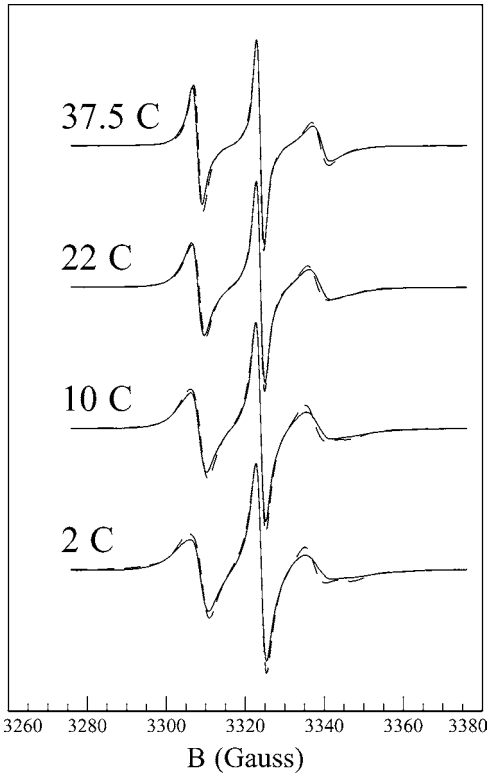

Figure 6. Nonlinear least-squares (NLLS) fits of the two-site SRLS model (dashed lines) to the experimental spectra (solid lines) at 9 GHz of T4 lysozyme in solution, spin-labeled at position 131. The best parameters from multifrequency fits are presented in Table 3.

rotational diffusion was used for convenience. The values of rotational diffusion tensor are in the range of $1 \times 10^5 - 3 \times 10^6$ s^{-1}, consistent with the (near) rigid limit. The g tensor results in Table 1 show that g_{xx} is slightly lower for 131R1 than for 72R1, whereas the reverse is true for A_{zz}. These trends are consistent with 131R1 experiencing a more polar environment than 72R1.[32,33]

4. Results

The experimental 250 and 9 GHz ESR spectra of T4 lysozyme mutants 131R1 and 72R1 are displayed in Figures 5−8. The results of simultaneously fitting the spectra at both frequencies to the SRLS model are presented in Table 3 as well as in Figure 9. The definitions of the various fitting parameters in the table are given in section 2. In the simultaneous fitting, all the dynamic and potential parameters used are the same for the spectra at both frequencies. We did, however, allow for differences in the (Gaussian) inhomogeneous broadening at the two frequencies. We typically find somewhat larger broadening for the 250 GHz spectra as expected, (e.g., ca. 2 G vs 1 G for 250 GHz vs 9 GHz for 131R1 and ca. 1.4 G vs 1 G for 72R1).

Columbus et al.[4] in their 9 GHz study did find that there are two components at lower temperatures, but not at room temperature, for 131R1. Our study also indicated the presence of two components, so we allowed for the presence of two components in our simultaneous analysis of the spectra at the two frequencies. Indeed, we find that two components are present for 131R1 at lower temperatures, but not at the highest temperature. (Note that the two-component fits led to significantly reduced chi-squared values at the lower temperatures.) The existence of the two components has been tentatively ascribed to a weak interaction of the ring with the protein environment.[4]

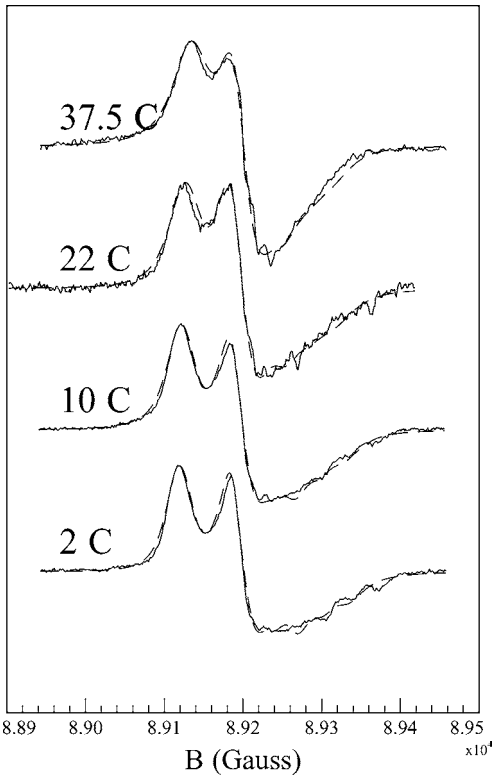

Figure 7. Nonlinear least-squares (NLLS) fits of the two-site SRLS model (dashed lines) to the experimental spectra (solid lines) at 250 GHz of T4 lysozyme in solution, spin-labeled at position 72. The best parameters from multifrequency fits are presented in Table 3.

Initially, the fitting was performed with the admixture of the two components constrained to a common value for both 9 and 250 GHz. However, we could not obtain good fits until we

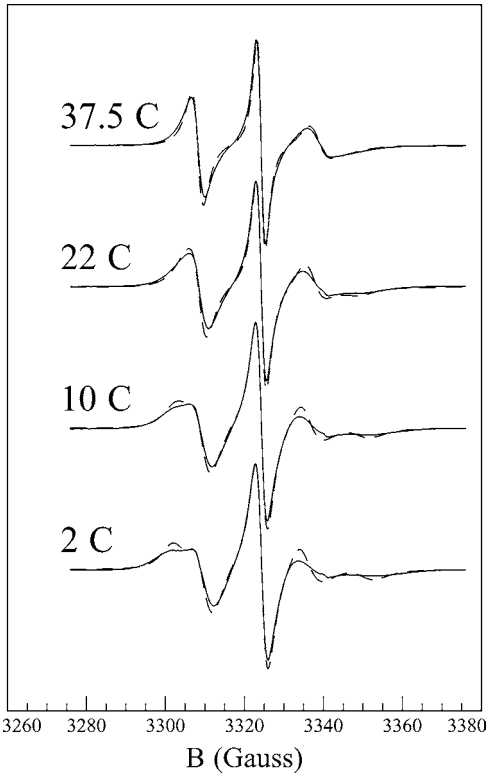

Figure 8. Nonlinear least-squares (NLLS) fits of the two-site SRLS model (dashed lines) to the experimental spectra (solid lines) at 9 GHz of T4 lysozyme in solution, spin-labeled at position 72. The best parameters from multifrequency fits are presented in Table 3.

TABLE 1: Magnetic Tensor Parameters[a,b]

mutant site	g_{xx}	g_{yy}	g_{zz}	A_{xx} (G)	A_{yy} (G)	A_{zz} (G)
131	2.007 79	2.005 78	2.002 21	5.00	5.00	36.85
72	2.008 03	2.005 82	2.002 18	6.42	5.95	35.83

[a] The estimated relative error in the g tensor components is $\pm 5 \times 10^{-6}$. [b] The estimated error in A tensor components is ± 0.2 G.

TABLE 2: Global Diffusion Rates of T4 Lysozyme[a]

t (°C)	$R^c(10^7\ s^{-1})$ (used in Table 3)	$R^c(10^7\ s^{-1})$ (from independent estimates)
2	1.21	1.47
10	1.48	1.90
22	1.78	2.73
37.5	2.75	4.18

[a] Note that the correlation time, τ_c, for overall tumbling is given by $\tau_c = (6R^c)^{-1}$.

allowed for different admixtures of the two components at the two frequencies. In general, for 131R1 the differences were negligible to moderate, and at 37.5 °C the two-component fitting routine unequivocally returned the presence of only a single component at both frequencies. In the case of 72R1, the 9 GHz spectra show only a negligible second component consistent with previous work,[4] but the 250 GHz results yield a more substantial second component at the lower temperatures. However, the fitting yields only a single component for both frequencies at and above room temperature. (Note that Barnes et al. in their study of different T4 lysozyme mutants,[13] using the simpler fitting procedure (outlined above), wherein the spectrum at each frequency was fit separately, also obtained different admixtures of the two components.)

It should be noted that the populations of the two components are fit in a simple linear least squares manner, unlike the other parameters in Table 3 which require nonlinear least-squares fitting.[23] Thus, they cannot be preset (or seeded with any initial values) and must be allowed to float in the computation. We have found, in the course of many fittings and simulations of two-component spectra at a single frequency, that the precise values of the populations of the two components are quite sensitive to the choice of the other fitting parameters. Thus, the fact that differences do show in the results at the two frequencies is likely an indication of small imperfections in the overall fitting. They can arise from the abundance of parameters to fit in the presence of more than one component. In particular, component 2 is present in low concentration, so its fitting parameters are somewhat less accurate. In fact, in those fits where we constrained the populations P to a common value at both frequencies, the parameters obtained for the more prevalent component 1 were within a few percent of those in Table 3, whereas some of those for component 2 were substantially changed.[34] Thus, we regard the fits to component 1 to be more reliable.

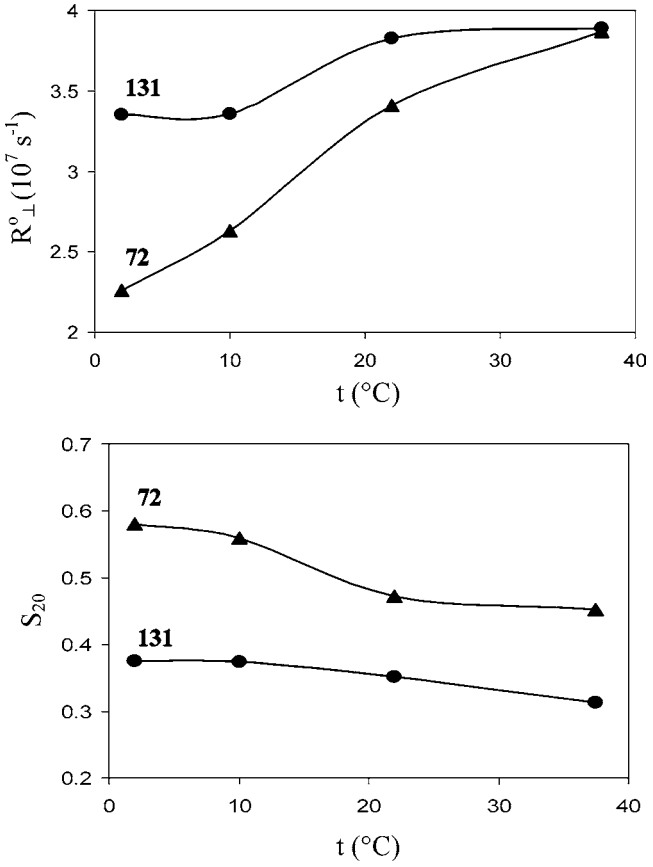

Figure 9. Temperature dependence of $R^o_\perp$ and S_{20} for the dominant component.

We wish to emphasize that the higher temperature results, which unequivocally return a single component 1, are clearly the most reliable. Furthermore, they lead to good simultaneous fits at both frequencies. Given this observation, as well as those that (i) at the lower temperatures the results for the dominant component 1 were hardly affected by which method was used for fitting populations and (ii) we obtained consistent results as a function of temperature for the various parameters (which is useful in mitigating against ambiguity in fitting ESR spectra[35,36]), we regard the results on component 1 to be reliable and appropriate for further analysis. Figure 9 compares the results on $R^o_\perp$ and c_{20} vs temperature for component 1 of 72R1 and 131R1.

As we have just noted, the spectra at both frequencies could be simultaneously fit quite satisfactorily at the higher temper-

TABLE 3: Simultaneous Multifrequency SRLS Best Fit Results for T4 Lysozyme[a]

t (°C)	comp	$R^o_\perp$ (10^8 s^{-1})	$R^o_\parallel$ (10^7 s^{-1})	c_{20}	c_{22}	R^c (10^7 s^{-1})	P_9 (%)	P_{250} (%)	S_{20}	S_{22}	W_9 (G)	W_{250} (G)
						131R1						
2	1	3.35	2.24	1.71	−0.31	1.21	81	83	0.375	−0.056	1.13	1.99
	2	0.259	3.72	2.03	−2.20	1.21	19	17	0.412	−0.146		
10	1	3.36	2.84	1.69	−0.25	1.48	94	79	0.374	−0.049	0.99	2.03
	2	0.262	4.47	1.96	−1.42	1.48	6	21	0.338	−0.259		
22	1	3.83	3.98	1.59	−0.15	1.78	93	82	0.352	−0.032	0.72	2.01
	2	0.347	5.72	1.78	−1.10	1.78	7	18	0.335	0.216		
37.5	1	3.89	4.48	1.42	−0.25	2.75	100.0	100.0	0.313	−0.058	0.56	1.04
						72R1						
2	1	2.26	2.00	2.93	−0.72	1.21	96	71	0.313	−0.058	0.56	1.04
	2	5.87	0.701	2.71	−2.52	1.21	4	29	0.350	−0.350		
10	1	2.63	2.51	2.80	−0.74	1.48	97	67	0.560	−0.082	0.91	1.38
	2	6.10	1.96	2.46	−2.06	1.48	3	33	0.365	−0.308		
22	1	3.41	3.26	2.24	−0.54	1.78	100.0	100.0	0.472	−0.082	0.84	1.43
37.5	1	3.87	4.89	2.16	−0.63	2.75	100.0	100.0	0.452	−0.100	0.51	0.37

[a] The errors are estimated to be ±2% for both $R^o_\perp$ and $R^o_\parallel$ and ±1% and ±12% for c_{20} and c_{22} respectively; see text.

TABLE 4: Correlation Matrices of Fitting Parameters Using SRLS Model

	$R^o_\perp$	$R^o_\parallel$	c_{20}	c_{22}
		250 and 9 GHz		
$R^o_\perp$	1.00	−0.28	0.11	0.49
$R^o_\parallel$		1.00	0.16	0.22
c_{20}			1.00	0.87
c_{22}				1.00
		250 GHz Only		
$R^o_\perp$	1.00	−0.60	0.90	−0.22
$R^o_\parallel$		1.00	0.55	−0.27
c_{20}			1.00	−0.28
c_{22}				1.00
		9 GHz Only		
$R^o_\perp$	1.00	0.60	0.82	−0.55
$R^o_\parallel$		1.00	0.32	−0.86
c_{20}			1.00	−0.27
c_{22}				1.00

atures wherein only a single component was present, but there was some difficulty in the fitting at the lower temperatures when two components are present. This suggests that there might be a key feature or mechanism, not included in our analysis, that is present when there are two components but which is not relevant for just a single component. One such possibility is that there is dynamic exchange occurring between the two conformers yielding the two spectral components. It could have different effects on the spectra at the two frequencies given their different time scales. For example, the exchange rate could be slow on the 250 GHz scale, leading to just relatively small broadening of the already broad spectra, whereas at 9 GHz the nearly motionally narrowed spectra are likely to be more similar, so that the exchange may possibly lead to some exchange narrowing. A careful analysis of effects of exchange on slow-motional ESR spectra at different frequencies awaits a proper theoretical analysis, which is currently under development.

To study the correlations and errors in the fitting parameters, the correlation matrices for these parameters are shown in Table 4 for site 72 at 22 °C. For comparison, the single-component spectra were fit in several ways: (1) a simultaneous fit for 250 and 9 GHz, (2) a separate fit for 250 GHz, and (3) a separate fit for 9 GHz. (In all these cases, R^c was fixed at the optimum value as discussed below). Two fitting parameters are usually considered to be strongly correlated with each other if the correlation coefficient between them is larger than 0.9. For instance, there is a strong correlation between $R^o_\perp$ and c_{20} in the 250 GHz separate fit (case 2), as can be seen in Table 4. The same is observed from the 9 GHz separate fit (case 3). However,

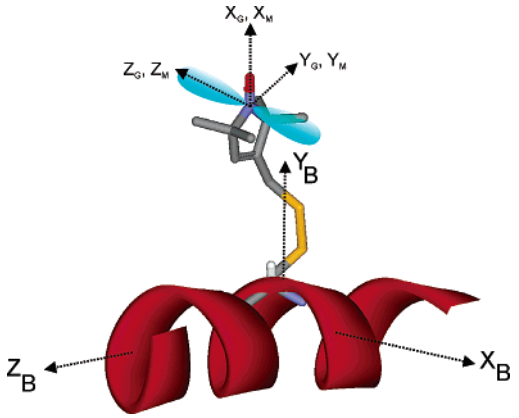

Figure 10. Schematic illustration of a decomposition of the coordinates for internal motion represented by the R^o tensor with frame X_M, Y_M, Z_M into the internal motion of the tether with frame X_G, Y_G, Z_G and fluctuations in the helix (with frame X_B, Y_B, Z_B) to which it is attached.

this strong correlation is removed when the simultaneous fit is performed (case 1), as the results in Table 4 indicate. We find that in nearly all cases the correlation coefficients are significantly reduced for case 1. This may be regarded as further support to the multifrequency ESR approach.

Finally, the fitting errors of each parameter are also listed in Table 3. The error estimates were obtained by repeatedly fitting the spectra using different sets of seed values of the variables. From the distribution in values obtained, the errors could be estimated for each parameter. We regard this as a more robust method of estimating error than the standard method described by Budil et al.,[23] which yielded error estimates that are generally smaller.[37]

In our analysis, we found that the use of fully anisotropic local diffusion tensors for the internal motion,[4,13,23,24,26] instead of axially symmetric tensors (i.e., $R^o_{xx} \neq R^o_{yy}$ instead of $R^o_{xx} = R^o_{yy} = R^o_\perp$), did not lead to significantly improved fits to the experiments but, on the other hand, led to unnecessarily large correlations between these (and other) parameters, indicating an excess number of parameters to be fit. As a result, we limited the fitting to $R^o_\perp$ and $R^o_\parallel$ ($= R^o_{zz}$). This amounts to setting $R^o_\perp = (1/2)(R^o_{xx} + R^o_{yy})$ and letting $(R^o_{xx} - R^o_{yy}) \simeq 0$. As in the previous multifrequency study on other T4L mutants,[13] we found that the primary or z axis of local diffusion (corresponding to R^o_{zz}) is best taken as parallel to the z axis of the nitroxide magnetic tensors (corresponding to g_{zz} and A_{zz}) (cf. Figure 10).

From the dynamic and ordering parameters for the local dynamics vs temperature shown in Figure 9 for component 1,

it is seen that their temperature variation is consistent with the expected increase in motional rates and decrease in local ordering with temperature. Clearly, there are differences in the local dynamic and ordering parameters for the two mutants, which we discuss in detail below. However, one certainly expects that their respective overall tumbling rates, R^c, are the same. The results shown in Table 3 were obtained by constraining the R^c to be the same for both 131R1 and 72R1. Initially we seeded the values of R^c in the fitting based on the value of R^c previously measured for T4 lysozyme at 20 °C, wherein a value of 2.6×10^7 s^{-1} was obtained.[38] Estimated values for R^c were obtained at the other temperatures by scaling this experimental result using the viscosity of water[39] and Stokes−Einstein hydrodynamic theory for which

$$R^c = \frac{k_B T}{8\pi r^3 \eta} \tag{15}$$

where T is the temperature and r is the hydrodynamic radius of T4 lysozyme. Whereas the use of this independently measured (and scaled) set of R^c values led to good fits for 131R1, it proved less satisfactory for fitting the spectra from 72R1. We found it necessary to reduce R^c somewhat in order to get good fits to both 72R1 and 131R1 with the same R^c. These values of R^c appear in Table 3, and they are compared with the "independent" values in Table 2. They range from 82% of the latter value at 2 °C to 66% at 37.5 °C. We regard this as quite reasonable agreement, considering different experimental methods and possible differences in sample preparation. (In fact, other workers have obtained a range of values.[40])

To obtain further insights to compare with this approach, we performed separate least-squares fitting of 131R1 and of 72R1 wherein we let R^c vary independently for each mutant. We found that for 131R1 the resultant values of R^c are close to those in Table 3, whereas those for 72R1 are about 70% of these values, a matter that we discuss further below. Of greater significance, we find that the fits, using this approach, to the dynamic and ordering parameters for the local dynamics for the two mutants are generally very close to those shown in Table 3. Thus, the graphs in Figure 9 would only be slightly affected, and the significant observations we discuss below are unaffected.

One observes from Figures 5−8 that the agreement between theory and experiment is generally good for both sites at the different temperatures.

5. Analysis and Discussion

A primary objective of this study is to show how the multifrequency ESR approach can successfully determine differences between local dynamics of R1 at different sites. The comparison of 250 GHz spectra in Figure 3 clearly shows that there must be significant differences between 131R1 and 72R1. The differences in their local motions are emphasized partly because these spectra are only slightly affected by the slow overall tumbling. The results of our analysis, summarized in Figure 9 for the dominant component, show that 72R1 displays significantly greater local ordering than does 131R1 (e.g., an S_{20} of 0.47 vs 0.35 at 22 °C). In general, 72R1 exhibits somewhat slower local dynamics than 131R1 as reported by $R_\perp^o$, but this difference is negligible at the higher temperatures. This observation is consistent with that of Columbus et al.[4] based on their 9 GHz study using the MOMD model. In fact, they also obtain respective values of S_{20} of 0.47 and 0.35, which is remarkable agreement considering their substantially different analysis. (Note that their study used solutions containing 30% sucrose, which reduced the importance of overall tumbling on the 9 GHz spectra, and among other things they utilized a substantial "diffusion tilt" angle of 36°.)

Columbus et al. point out that there are no tertiary interactions at either site, so this should not differentiate them. Instead, they propose that the mobility difference reflects dynamic differences in the helical backbone itself arising from structural and environmental differences between their respective helices. They summarize these differences as follows: ".. the 131 helix consists of only two and a half-turns, hardly long enough for end effects to decay at the central 131 site.. On the other hand, site 72 is located in the center of a long 5-turn helix. The 72 helix has a stabilizing threonine N-cap, while the 131 helix has two positively charged residues in the N-capping box, which are poor helix caps. Perhaps most importantly, the segment of the helix that contains site 72 is located near the tightly packed hydrophobic core of a helix bundle." They suggest that these features, as well as higher Debye−Waller factors and H exchange rates at 131 as compared to 72, may indicate larger amplitude backbone fluctuations near 131 "due to an intrinsically lower thermodynamic stability of the secondary structure."

Our results, heavily dependent on the greater sensitivity of 250 GHz ESR spectra to the local dynamic structure, lend further support to this hypothesis. Thus, while the overall restriction to amplitude of motion of the nitroxide is a composite of the restricted motion about its tether and the restrictions of the backbone fluctuations, it would appear from these considerations that the latter is an important contributor to the difference between the two mutants.

In other respects, however, our multifrequency SRLS analysis yields results that differ. Most significant is the large values of $R_\perp^o$ obtained for both 72R1 and 131R1 and shown in Figure 9, as compared to the values of $R_\parallel^o$ (cf. Table 3). We observe for the dominant component that $R_\perp^o$ is about an order of magnitude greater than $R_\parallel^o$ for both mutants over the whole temperature range studied. This is quite similar to the results of Barnes et al.[13] using both 250 and 9 GHz spectra on different mutants of T4L (i.e., sites 44R1 and 69R1). They noted that this is a consequence of using the spectra at both frequencies in their analysis, whereas if a nonlinear least-squares fitting is performed on just the 9 GHz ESR spectra using a MOMD model that ignores the contribution of the overall tumbling, one typically finds parameters wherein $R_\parallel^o$ is much greater than $R_\perp^o$, or the reverse of what has been found using both frequencies. Columbus et al. obtained values from the MOMD model wherein the rotational diffusion tensor components are more nearly equal, from their samples with greater viscosity in sucrose/water solutions. At present, we do not yet understand the origin of the apparent rate differences, but it could be due, in part, to higher resolution at 250 GHz.

Barnes et al. suggested that the larger $R_\perp^o$ may be due to the motion of the peptide backbone to which the spin probe is attached. This is schematically illustrated in Figure 10, which shows an expected conformation of the spin-label side chain attached to a helical sequence.[41] It shows the principal axis system of the nitroxide magnetic tensors (labeled X_G, Y_G, Z_G), as well as those for the internal rotational diffusion (and ordering) tensors (labeled X_M, Y_M, Z_M), are parallel according to our spectral fitting, as we have discussed above. These axes perhaps best represent the motional properties of the nitroxide label itself, especially its internal rotation about the two bonds of its tether most immediate to the pyrroline ring containing the nitroxide. To consider the backbone motions of the helix, we suggest a principal axis system for the helix (X_B, Y_B, Z_B),

such that Z_B is along the principal axis of the helix and X_B is nearly parallel to Z_M. The cylindrical symmetry of the helix suggests that its local fluctuations would be represented by an axially symmetric diffusion tensor D_i^b, $i = X_B, Y_B, Z_B$ with $D_{X_B}^b = D_{Y_B}^b = D_\perp^b$ and $D_{Z_B}^b = D_\parallel^b$. The internal motion of the pyrroline ring about its tether may similarly be described by local diffusion tensor D_i^g, $i = X_G, Y_G, Z_G$. Let us assume for convenience that each compoment, R_i^o ($i = xx, yy, zz$), of the internal rotation tensor, which is extracted from the experimental analysis, can be approximated as a simple sum over the two types of internal motion about their respective axes. This yields $R_\parallel^o \simeq D_Z^g + D_\perp^b$ and $R_\perp^o \simeq (1/2)(D_X^g + D_Y^g + D_\perp^b + D_\parallel^b)$. Given that rotations about the fourth bond in the tether have a greater amplitude than rotations about the fifth bond, due to steric constraints,[4,7,13] Barnes et al.[13] considered tether motion about Z_G to be fastest, yielding $D_Z^g = D_\parallel^g > D_\perp^g = D_X^g \simeq D_Y^g$. Given our observation that $R_\perp^o \gg R_\parallel^o$, it would follow that $D_\parallel^b$ is a dominant contributor to $R_\perp^o$ and also $D_\parallel^b \gg D_\perp^b$. On the other hand, Columbus et al., using spin-labels with different substituents, present evidence that rotation about the last bond "is the major contributor to spectral averaging", and this approximately corresponds to tether motion about X_G. This latter possibility would also yield an $R_\perp^o \gg R_\parallel^o$.

Clearly further studies are required to clarify this issue. Columbus et al. showed the use of 4-substituted derivatives of the pyrroline ring suppresses the internal motions of that ring about the tether, so it would be helpful to perform multifrequency studies using these modified spin-labels to compare with the results in this work.

Finally, we would like to mention the possibility that in our least-squares fitting to SRLS the preference for a smaller R_c for 72R1 than for 131R1 might be the manifestation of slow backbone modes occurring over the same slow time scale as the overall tumbling, and therefore affecting the "apparent" overall tumbling rate. This would imply that the greater value of R_c for 131R1 results from its greater helix flexibility as discussed above. Further studies, possibly over a range of several ESR frequencies, might help to differentiate the various dynamic processes beyond what can be achieved using two frequencies and the two-dynamic-mode SRLS model, as we have done in this study.

6. Summary and Future Prospects

This work illustrates how multifrequency ESR is a useful tool for studying dynamics of proteins. A challenging task in such studies is to deconvolute the various modes of motion. ESR spectra obtained at different frequencies enable one to open different time scale windows, so that processes with different correlation times can be selectively probed. In this work the analysis of 250 and 9 GHz ESR spectra using the SRLS model has enabled us to separate the slower global motion of T4 lysozyme from the faster internal motions by employing the SRLS model, which distinguishes these modes. This has allowed us to show that a nitroxide label on a long 5 turn helix exhibits greater internal motional restriction (i.e., increased local ordering) as compared to the same label on a shorter two and a half turn helix, which seems intuitively quite reasonable. The use of new software, which permits simultaneous fitting of the spectra at different frequencies, significantly aided in this analysis. Also, the enhanced resolution of very high-frequency ESR (250 GHz) to the internal dynamics clearly showed that it must differ at the two labeled sites by virtue of the qualitatively different spectra obtained.

Nevertheless, at this stage of development of multifrequency ESR studies of protein dynamics, it is not yet possible to unambiguously distinguish between contributions of slower internal modes of motion (e.g., slow backbone modes) from the slow overall tumbling or to distinguish faster backbone modes from the restricted internal motions of the nitroxide about its tether, although there are suggestions of such effects in our results. It should be possible to improve on the current study and methodology to address such issues along several distinct, but complementary, avenues of approach. First of all, spectra taken at three or more ESR frequencies would enhance the data set from which to extract the dynamics of the different modes utilizing the new software. Second, Columbus et al.[4] have introduced newer spin-labels which suppress the internal motions of the nitroxide about its tether, and these would be valuable to use in the multifrequency studies. It could also be useful to suppress the overall tumbling motion by such methods as an increase in solvent viscosity.[4] It is our intention to implement such improvements in further studies.

In addition, improved models may be needed to interpret the more extensive data. It would be desirable to more accurately model the internal motions of the protein, the nitroxide internal motions, and the overall tumbling. A useful tool to gain insight into these is by molecular dynamics (MD) simulations. It can provide trajectories of the probe and protein motions and their interactions with the solvent over the time scale of picoseconds to nanoseconds. In fact, very recently Stoica[43] has performed MD to simulate the ESR spectra of spin-labeled T4 lysozyme. While at present these simulations were not very successful at reproducing typical 250 GHz ESR spectra, one might expect future developments will be more successful. One challenge is to provide long enough trajectories.[43,44] Stoica attempted to address this by combining 10 MD trajectories of 5.5−6 ns each, but unfortunately this was not sufficient to yield correlation functions that reach equilibrium for the internal motions (the overall motion had been factored out). Another challenge would arise in the need to extensively repeat such MD trajectories if one were to attempt to fit the ESR spectra in a least-squares fashion, as is currently done using the SLE and as we have done in the present study. (In MD, one would need to vary force-field parameters.) Since the computation of each trajectory is extremely time-consuming, this is unrealistic. However, it is our belief that MD simulations can provide useful insight into determining what are the dominant internal modes of motion that contribute to the reorientational relaxation of the spin-label. Then, utilizing well-developed methods,[42] one can hope to construct even more appropriate stochastic models than the SRLS model (utilized in this work), which incorporate these dominant modes. These models could then be more efficiently utilized in fitting their relevant motional and ordering parameters to the ESR spectra.

Acknowledgment. This work was supported by National Institutes of Health grants RR016292 (J.H.F.), GM25862 (J.H.F.), and EY05216 (W.L.H.) and the Jules Stein Professorship Endowment (W.L.H.). The computations were performed at the Cornell Theory Center. J.H.F. thanks Professor Ron Elber for helpful discussions on MD simulations for ESR spectra.

References and Notes

(1) Kay, L. E. *Nat. Struct. Biol.* **1998**, *5*, 513−516.
(2) Ishima, R.; Torchia, D. A. *Nat. Struct. Biol.* **2000**, *7*, 740−743.
(3) Parak, F. G. *Curr. Opin. Struct. Biol.* **2003**, *13*, 552−557.
(4) Columbus, L.; Kalai, T. K.; Hideg, J. J. K.; Hubbell, W. L. *Biochemistry* **2001**, *40*, 3828−3846.

(5) Hubbell, W. L.; Cafiso, D. S.; Altenbach, C. *Nat. Struct. Biol.* **2000**, *7*, 735−739.

(6) Hubbell, W. L.; Gross, A.; Langen, R.; Lietzow, M. A. *Curr. Opin. Struct. Biol.* **1998**, *8*, 649−656.

(7) Columbus, L.; Hubbell, W. L. *TIBS* **2002**, *27*, 288−295.

(8) Liang, Z.; Freed, J. H. *J. Phys. Chem. B* **1999**, *103*, 6384−6396.

(9) Meirovitch, E.; Nayeem, A.; Freed, J. H. *J. Phys. Chem.* **1984**, *88*, 3454−3465.

(10) Polnaszek, C. F.; Freed, J. H. *J. Phys. Chem.* **1975**, *79*, 2283−2306.

(11) Freed, J. H. *J. Chem. Phys.* **1977**, *66*, 4183−4199.

(12) Polimeno, A.; Freed, J. H. *J. Phys. Chem.* **1995**, *99*, 10995−11006.

(13) Barnes, J. P.; Liang, Z.; Mchaourab, H. S.; Freed, J. H.; Hubbell, W. L. *Biophys. J.* **1999**, *76*, 3298−3306.

(14) Tugarinov, V.; Liang, Z.; Shapiro, Y. E.; Freed, J. H.; Meirovitch, E. *J. Am. Chem. Soc.* **2001**, *123*, 3055−3063.

(15) Liang, Z.; Freed, J. H.; Keyes, R. S.; Bobst, A. M. *J. Phys. Chem. B* **2000**, *104*, 5372−5381.

(16) Lou, Y.; Ge, M.; Freed, J. H. *J. Phys. Chem. B* **2001**, *6*, 11053−11056.

(17) Borbat, P. P.; Costa-Filho, A. J.; Earle, K. A.; Moscicki, J. K.; Freed, J. H. *Science* **2001**, *291*, 266−269.

(18) Freed, J. H. In *EPR in the 21st Century*; Kawamori, A., Yamauchi, J., Ohta, H., Eds.; Elsevier Science: Amsterdam, 2002.

(19) Tugarinov, V.; Shapiro, Y. E.; Liang, Z.; Freed, J. H.; Meirovitch, E. J. *Mol. Biol.* **2002**, *315*, 155−170.

(20) Shapiro, Y. E.; Kahana, E.; Tugarinov, V.; Liang, Z.; Freed, J. H.; Meirovitch, E. *Biochemistry* **2002**, *41*, 6271−6281.

(21) Meirovitch, E.; Shapiro, Y. E.; Tugarinov, V.; Liang, Z.; Freed, J. H. *J. Phys. Chem. B* **2003**, *107*, 9883−9897.

(22) Meirovitch, E.; Shapiro, Y. E.; Liang, Z.; Freed, J. H. *J. Phys. Chem. B* **2003**, *107*, 9898−9904.

(23) Budil, D. B.; Lee, S.; Saxena, S.; Freed, J. H. *J. Magn. Reson.* **1996**, *120*, 155−189.

(24) Pilar, J.; Labsky, J.; Marek, A.; Budil, D. E.; Earle, K. A.; Freed, J. H. *Macromolecules* **2000**, *33*, 4438−4444.

(25) Poluektov, O. G.; Utschig, L. M.; Dalosto, S.; Thurnauer, M. C. *J. Phys. Chem. B* **2003**, *107*, 6239−6244.

(26) Freed, J. H. In *Spin Labeling: Theory and Applications*; Berliner, L., Ed.; Academic Press: New York, 1976; p 53.

(27) Schneider, D. J.; Freed, J. H. *Adv. Chem. Phys.* **1989**, *73*, 387.

(28) Schneider, D. J.; Freed, J. H. In *Biological Magnetic Resonance*; Berliner, L. J., Reuben, J., Eds.; Plenum Publishing: New York, 1989; Vol. 8.

(29) Copies of this new software may be obtained from the authors upon request.

(30) Barnes, J. P.; Freed, J. H. *Rev. Sci. Instrum.* **1997**, *68*, 2838−2846.

(31) Earle, K. A.; Budil, D. E.; Freed, J. H. *J. Phys. Chem.* **1993**, *97*, 13289−13297.

(32) Onder, M. A.; Grinberg, O. Ya.; Dubinskii, A. A.; Lehedev, Ya. S. *Sov. J. Chem. Phys.* **1985**, *3*, 781−792.

(33) Earle, K. A.; Moscicki, J. K.; Ge, M.; Budil, D. E.; Freed, J. H. *Biophys. J.* **1994**, *66*, 1213−1221.

(34) Note that when constrained to a common P, the values obtained for P were close to those given in Table 3 for P_9.

(35) Ge, M.; Freed, J. H. *Biophys. J.* **1999**, *76*, 264−280.

(36) Ge, M.; Freed, J. H. *Biophys. J.* **2003**, *85*, 4023−4040.

(37) We have also carried out fits of the 250 GHz spectra to the MOMD model to ascertain to what extent the internal motional parameters are affected by neglecting the slow overall tumbling motions in the MOMD model. Those obtained for the higher temperature, single-component spectra were compared with the results in Table 3. The differences in values were typically in the range of 5−15% for $R_{\perp}^{o}$, $R_{\parallel}^{o}$, and S_{20} but were as great as a factor of 2 in a few cases. The differences for S_{22} were 60−80%. We regard these as significant discrepancies arising from the use of the MOMD model.

(38) Brune, D.; Kim, S. *Proc. Natl. Acad. Sci. U.S.A.* **1993**, *90*, 3835−3839.

(39) *CRC Handbook of Chemistry and Physics*, 80th ed.; Lide, D. R., Ed.; CRC Press: Boca Raton, FL, 1999.

(40) Venable, R. M.; Pastor, R. W. *Biopolym. J.* **1988**, *27*, 1001−1014.

(41) Langen, R.; Oh, K.-J.; Cassio, D.; Hubbell, W. L. *Biochemistry* **2000**, *39*, 8396−8405.

(42) Polimeno, A.; Freed, J. H. *Adv. Chem. Phys.* **1993**, *73*, 387−528.

(43) Stoica, I. *J. Phys. Chem. B* **2004**, *108*, 1771−1782.

(44) Hakansson, P.; Westlund, P. O.; Lindahl, E.; Edholm, O. *Phys. Chem. Chem. Phys.* **2001**, *3*, 5311−5319.